A Linear Stability Analysis of Saltwater as Applied to Land Sea Ice

Katherine Roddy
Dartmouth College, Hanover, NH 03755, U.S.A.
katherine.s.roddy@dartmouth.edu

August 29, 2008

Abstract

We seek to investigate the next generation of mathematical models used to understand climate variability. We hope to further what little is understood about small scale flows within global climate models. Specifically, the flow of saltwater near ice is examined with a simple box model. Possible physical applications include flows within a crack found in land sea ice and flows found near an ice shelf and saltwater interface. The box model could also provide subgrid scale for larger land and ocean climate models. A linear stability analysis of the governing equations for saltwater is performed to quantify various flow regimes. Using a set of functions in MATLAB, a Chebyshev collocation method is used to reduce the resulting differential eigenvalue problem to a matrix eigenvalue problem. The solution of the matrix eigenvalue problem follows in MATLAB. Neutral stability curves and associated critical Grashof numbers and wavenumbers are supplied for parameters representing pure and saltwater near the freezing point. A graphical comparison of the growth rates for secondary flows found in pure water and saltwater is conducted.

1 Introduction

The use of a box model with differentially heated isothermal side walls to represent various fluid flows has been a popular technique in fluid dynamics for decades ((Batchelor, 1954), (Vest and Arpaci, 1969), (Bergholz, 1978)). Physical applications vary widely within both commercial (double paned windows, (Batchelor, 1954), e.g.) and scientific (oceanography, metallurgy, atmospheric science, vulcanology, etc.) settings. For the various fluids and geometric configurations of the model, the primary focus remains largely the same over time. The primary mode of heat transfer employed by a differentially heated fluid can be described by the value of a fluid parameter called the Rayleigh number, given by

$$Ra = Gr_T Pr \tag{1}$$

where Gr_T and Pr represent the thermal Grashof and Prandtl numbers, respectively:

$$Gr_T = \frac{g\beta_T \delta T h^3}{\nu} \tag{2}$$

$$Pr = \frac{\nu}{\kappa_T} \tag{3}$$

Here g is the acceleration due to gravity, β_T is the thermal expansion coefficient, δT is the difference between the two sidewall temperatures, h is the width of the fluid cavity, ν is the kinematic viscosity of

Investigators	Fluid	Pr	$Gr*$	$m*$	A
Batchelor (1954), theory	air	0.73	18700	n/a	∞
Vest & Arpaci (1969), theory	air	0.71	7800	2.65	∞
Vest & Arpaci (1969), experiment	air	0.71	8700	2.74	33.33
Bergholz (1978), theory	air	0.71	8920	2.76	33.33
Bergholz (1978), theory	water	6.7	15300	1.40	37.04
Bergholz (1978), theory	water	6.7	12000	2.00	25
Ruth (1979), theory	air	0.70	8041.422	2.810	∞
Ruth (1979), theory	water	7.0	7868.426	2.767	∞
McBain & Armfield (2003), theory	air	0.7	8041.4222	2.8098	∞
McBain & Armfield (2003), theory	water	7.0	7868.4264	2.7671	∞
Evans (to be submitted), theory	air	0.71	8040	2.80	∞

Table 1: Previous linear stability results, with values for the parameters Prandtl number (Pr), critical Grashof number ($Gr*$), critical wavenumber ($m*$), and aspect ratio ($A = L/h$).

the fluid, and κ_T is its thermal diffusivity. For pure water ice (0°), $Pr = 13.183$, and in saltwater (salinity 35%), $Pr = 13.234$, following the data of Kukulka et al. (1987) .

Previous results of linear stability analysis for a two-dimensional differentially heated vertical cavity are given in table 1. The first to use such a model and to define the mean velocity and mean temperature of the primary flow was Batchelor (1954) ; see figure 2(b).

In their seminal work examining the stability of natural convection, Vest and Arpaci (1969) employ just such a vertical cavity with a uniform horizontal temperature gradient. They perform both an eigenvalue analysis using the Galerkin method and an experimental analysis using a rectangular plexiglass frame with aluminum sidewalls. Vest and Arpaci focus primarily on the convection of air, finding both experimental and theoretical critical values.

Bergholz (1978) and Lauriat and Desrayaud (1985) , among others, argue for the inclusion of a vertical temperature gradient experimentally found in the core of the main circulating flow. Lauriat and Desrayaud conclude that the lack of a vertical temperature gradient in the work of Vest and Arpaci does not appreciably affect stability results for a wide range of parameter values.

Ruth (1979) expands the cavity to three dimensions and develops a power series-based solution method for the problem. In the Appendix of critical data, Ruth gives extensive linear stability data, providing critical values for fluids of Prandtl number $1E^{-5}$ to 10.0. Using the data of Ruth as a benchmark, McBain and Armfield (2003), (2004) employ a Chebyshev collocation method to examine fluids of various Prandtl numbers, focusing specifically on Prandtl numbers higher than 10 for which Ruth's power series method fails. We will employ the same Chebyshev collocation method in our analysis.

Ehrenstein and Peyret (1989), Quon and Ghil (1992), Hadji and Jin (1996), Mergui and Gobin (2000), Bennacer et al. (2001), and Mamou et al. (2001), among others, examine the case of double-diffusive convection with the inclusion of a concentration gradient. Many focus on the classical fluid dynamic problem, the Benard problem, (stability of a fluid heated from below).

Ehrenstein and Peyret find instabilities in saltwater in their exploration of the Chebyshev collocation method in a version of the method we use in our analysis, though only within a limited time scale. Quon and Ghil conduct a thorough examination of the oceans' thermohaline circulation while focusing primarily on the interaction of the Rayleigh number with salt flux. Though horizontal, the primary box model

employed–two hot sidewalls and a cold isotherm in the center creating two separate circulations as a part of the main flow–is somewhat similar to the physical situation of a crack in a sheet of land sea ice, albeit with a reversed temperature distribution. Hadji and Jin investigate convection as a result of heat trapped under a sheet of ice escaping through a polynya, an area of exposed water similar to a pond or lake contained in land. Their physical model, that of a fluid cooled from above rather than heated from below, is a twist on the classic Benard problem. From these studies, we find the following parameters most consistently used to model saltwater at 20°: $Pr = 7.0$ or 7.1, $Le = 80$ or 100, and $Ns = 0.32$ or 0.5, with Ns often found as a negative value corresponding to a concentration gradient which opposes the temperature gradient.

As an experimental motivation for the present work, we note Josberger and Martin (1981) who examine flows resulting from the melting of pure ice into a saline solution in a box-like laboratory apparatus. As their experimental set-up matches what might be happening in land sea ice, we adopt their configuration (see figure 1). The authors note the initial presence of a bidirectional, laminar flow and a transition to turbulent flow patterns. Photographs and diagrams of the cusped surface of the ice-saltwater interface following the effects of such turbulent, secondary flows are given without significant analysis. Roughly converted from exponential form, the parameters used to numerically model the flow are similar to those used in the present study: $Pr = 11$, $Le = 200$, $Sc = 2500$.

We will conduct an eigenvalue-based linear stability analysis to determine the neutral stability point of saltwater. The Rayleigh number defines the primary mode of heat transfer in a fluid: for Rayleigh numbers below a critical value, conduction; for Rayleigh numbers above a critical value, convection. When the fluid is in the conductive state, it exhibits a stable circulating flow, the shear flow depicted in figure 2(a). In the convective state, the fluid is unstable to secondary flows, small perturbations of the main flow grown into local circulations as shown in figure 3.2. In our linear stability analysis, we will find the critical Rayleigh number (critical Grashof number for a specified Prandtl number) and associated wavenumber at the neutral stability point between laminar (primary) and turbulent (secondary) flow.

Our box model is presented in section 2 below. Section 3 details the equations used and a derivation utilizing the streamfunction. In section 4, we will discuss the Chebyshev collocation method used to solve the eigenvalue problem in MATLAB with Dirichlet boundary conditions. Conclusions as well as implications for further work are discussed in section 5.

2 The Model

We will extend the classic vertical box model with isothermal, differentially heated sidewalls ((Vest and Arpaci, 1969), (Bergholz, 1978)) to include a horizontal concentration (salinity) gradient. As a possible physical application, we note this configuration follows the situation of the edge of a sheet of pure ice melting into saltwater (Josberger and Martin, 1981). We also note that such a box model could serve as an appropriate approximation of the arched shape of the ice-water interface of the refreezing cracks in first-year land-fast sea ice experimentally measured by Petrich et al., 2007 .

As depicted in figure 1, the domain is defined as $\Omega = [x, y] = [0 : h, 0 : L]$ with no-slip conditions at the edges of the domain and insulating (adiabatic) top and bottom sidewalls held at constant temperature and concentration. We define the horizontal temperature and salinity gradients to be the same irrespective of their vertical location within the cavity, and the Boussinesq approximation is assumed to hold. Thus, the boundary conditions are:

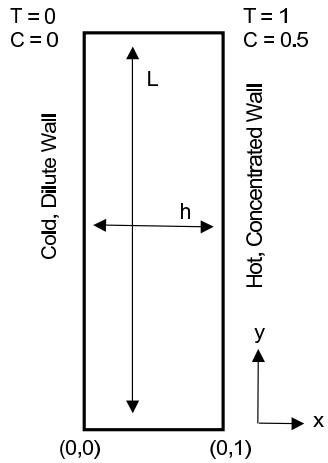

Figure 1: The box model. L is the height of the cavity in the y direction, and h is the width of the cavity in the x direction. The equations are nondimensionalized for a domain of $x = [0, +1]$.

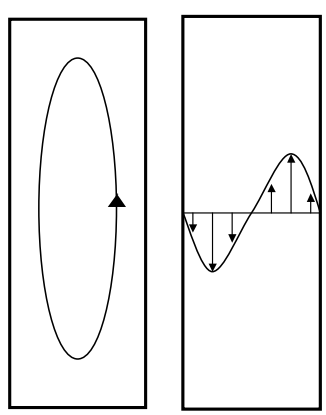

Figure 2: A schematic of the primary circulating flow in an infinite vertical cavity. (a) The buoyancy-driven, temperature-dominated counterclockwise circulation. (b) A solution for the mean velocity, $\bar{v} = \frac{1}{6}(x^3 - 1.5x^2 + 0.5x)$, over the domain $x = [0, +1]$ (Batchelor, 1954).

$$
\begin{aligned}
u = v =& 0, \quad \text{on} \quad \partial\Omega, \\
T(0,y) = T_l, \quad T(h,y) = T_r, \quad C(0,y) =& C_l, \quad C(h,y) = C_r, \quad y \in [0,L], \\
\frac{\partial T(x,0)}{\partial y} = \frac{\partial T(x,L)}{\partial x} = 0, \quad \frac{\partial C(x,0)}{\partial y} =& \frac{\partial C(x,L)}{\partial x} = 0, \quad x \in [0,h].
\end{aligned} \tag{4}
$$

As briefly described in section 1, in an infinitely high cavity, the main flow can be approximated as a shear flow where the effects of the ends of the cavity (the changing of the direction of the flow) can be ignored. As first described by Batchelor, a numerical solution for the mean velocity is found by examining the roots of the curve depicted in figure 2(b):

$$
\begin{aligned}
\bar{v} &= c \cdot x(x-0.5)(x-1) \\
\bar{v} &= c \cdot (x^3 - 1.5x^2 + 0.5x)
\end{aligned} \tag{5}
$$

The value used for the mean velocity is dependent upon the defined domain of the problem. Following the nondimensionalization defined in section 3, $c = 1/6$. The primary flow is buoyancy-driven and travels in a counterclockwise direction based on the setup of the box model in figure 1, following the uniform horizontal temperature gradient. Because the diffusivity of heat is much greater than that of salt, the buoyancy-driven flow is temperature-dominated: the heated fluid rises along the right wall of the cavity while the cooled fluid falls along the cavity's left wall, even as the salinity buoyancy force opposes such a flow.

3 Governing Equations and Derivation

3.1 Equations

The governing equations for saltwater are the Navier-Stokes equations, the continuity equation, and the conservation equations for temperature and concentration, here nondimensionalized for $t = \frac{t'h^2}{\nu Gr}$, $x = x'h$, $p = \frac{p'\rho\nu^2 Gr^2}{h^2}$, $T = T'\delta T$, and $C = C'\delta C$. The primes denoting nondimensionalization have been dropped, and the Grashof and Prandtl numbers, as introduced in section 1, have been incorporated:

$$
\frac{\partial u}{\partial t} + \nabla \cdot (\vec{u}u) - \frac{1}{Gr}\Delta u + \frac{\partial p}{\partial x} = 0 \tag{6}
$$

$$
\frac{\partial v}{\partial t} + \nabla \cdot (\vec{u}v) - \frac{1}{Gr}\Delta v + \frac{\partial p}{\partial y} = \frac{1}{Gr}T + \frac{1}{NsGr}C \tag{7}
$$

$$
\nabla \cdot \vec{u} = 0 \tag{8}
$$

$$
\frac{\partial T}{\partial t} + \nabla \cdot (\vec{u}T) - \frac{1}{GrPr}\Delta T = 0 \tag{9}
$$

$$
\frac{\partial C}{\partial t} + \nabla \cdot (\vec{u}C) - \frac{1}{NsGrLePr}\Delta C = 0 \tag{10}
$$

Here the velocity vector is denoted $\vec{u} = (u, v)$ where u and v are its x- and y-components, respectively. The (x, y) coordinate system is oriented as defined in figure 1. Pressure is p, temperature is T, concentration

(salinity) is C, and time is t. Δ represents the Laplacian operator, and ∇ represents the differential operator.

With the inclusion of an equation for concentration above, the introduction of two more fluid parameters is necessary. The Lewis number (Le) and the pseudo-Nusselt number (Ns), a parameter implemented to play the role of the Nusselt number without the difficult fractional exponent (Mergui and Gobin, 2000), are used here as conversion factors such that our analysis may focus on varying the value of the thermal Grashof number for one value of the thermal Prandtl number, as discussed in section 1. Thus we define Ns as the ratio of the solutal (Gr_C) and thermal (Gr_T) Grashof numbers, where β_C represents the salinity expansion coefficient, δC represents the difference in concentration between the two sidewalls, and all other parameters are defined as in section 1:

$$Ns = \frac{Gr_C}{Gr_T} = \frac{\beta_C \delta C}{\beta_T \delta T} \tag{11}$$

Similarly, the Lewis number is defined as the ratio of thermal diffusivity (κ_T) to solutal diffusivity (κ_C):

$$Le = \frac{\kappa_T}{\kappa_C} \tag{12}$$

For consistency, we use the data of Kukulka et al. for the situation of ice (0°) in saltwater (35% salinity): $\beta_C = 78.067E^{-5}/\%$, $\beta_T = 50.22E^{-6}/°C$. Kukulka et al. gives data for the Schmidt number, $Sc = LePr$, rather than for the Lewis number, though only at a salinity of 28.5%: $Sc = 2654.9$.

Therefore, as in equations (6) - (10), Gr and Pr should be read as the *thermal* Grashof and Prandtl numbers, and $Gr_C = NsGr$, $Pr_C = LePr$ have been substituted throughout for simplicity.

3.2 Perturbation Analysis

Following linear stability theory and the work of Vest and Arpaci, among others, mathematically we examine whether a perturbation will grow into an instability of the main flow. Each of the dependent variables u, v, p, T, and C is expressed as a sum of the mean and a perturbation of the mean, where η is some dependent variable:

$$\eta = \bar{\eta} + \eta' \tag{13}$$

The resulting expressions are substituted into equations (6) - (10) and simplified using the following assumptions, motivated by our physical understanding of the primary circulating flow given in figure 2:

$$\begin{aligned} \bar{u} &= 0, \\ \bar{v} &= \frac{1}{6}(x^3 - 1.5x^2 + 0.5x), \\ \bar{T} &= 1x, \\ \bar{C} &= 0.5x. \end{aligned} \tag{14}$$

Thus, the mean v, T, and C values depend only on x, and both $\bar{T}$ and $\bar{C}$ disappear for derivatives of degree two or higher. To linearize, any term which contains a perturbation multiplied by another

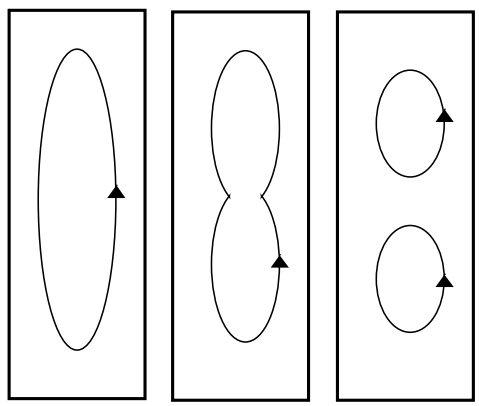

Figure 3: A conceptualization of the effects of γ on the fluid flow. (a) is the conduction regime, $\gamma < 0$, where the flow is parallel to temperature and concentration isobars. (b) captures the growth of a perturbation into a bifurcation (division) of the primary flow. (c) depicts the convection regime, $\gamma > 0$, where a secondary flow regime is prescribed. Within the range of $\gamma > 0$, real values of γ define the oscillations (movements throughout the cavity in time) of the flow, and imaginary values of γ define the rate of perturbation growth or decay.

perturbation is ignored. Incorporating the perturbation variables, assumptions, and utilizing the continuity equation, we find:

$$\frac{\partial u'}{\partial t} + \bar{v}\frac{\partial u'}{\partial y} - \frac{1}{Gr}\Delta u' + \frac{\partial p'}{\partial x} = 0 \tag{15}$$

$$\frac{\partial v'}{\partial t} + \bar{v}\frac{\partial v'}{\partial y} + u'\frac{\partial \bar{v}}{\partial x} - \frac{1}{Gr}\Big(\Delta v' + \frac{\partial^2 \bar{v}}{\partial x^2}\Big) + \frac{\partial p'}{\partial y} - \frac{1}{Gr}(\bar{T} + T') - \frac{1}{NsGr}(\bar{C} + C') = 0 \tag{16}$$

$$\frac{\partial u'}{\partial x} + \frac{\partial v'}{\partial y} = 0 \tag{17}$$

$$\frac{\partial T'}{\partial t} + \bar{v}\frac{\partial T'}{\partial y} + u'\frac{\partial \bar{T}}{\partial x} - \frac{1}{GrPr}\Delta T' = 0 \tag{18}$$

$$\frac{\partial C'}{\partial t} + \bar{v}\frac{\partial C'}{\partial y} + u'\frac{\partial \bar{C}}{\partial x} - \frac{1}{NsGrLePr}\Delta C' = 0 \tag{19}$$

Equations (15) - (19) match Evans , and the addition of equation (19) follows equation (18).

3.3 Introduction of the Streamfunction

Conceptualizing a snapshot of the velocity field of a fluid at a particular instant results in a series of streamlines of the fluid. These lines are constructed by the streamfunction, ψ', whose partial derivatives with respect to x and y are taken to represent the y- and x-components of the perturbation velocity vector, respectively:

$$u' = -\frac{\partial \psi'}{\partial y}, \quad v' = \frac{\partial \psi'}{\partial x} \tag{20}$$

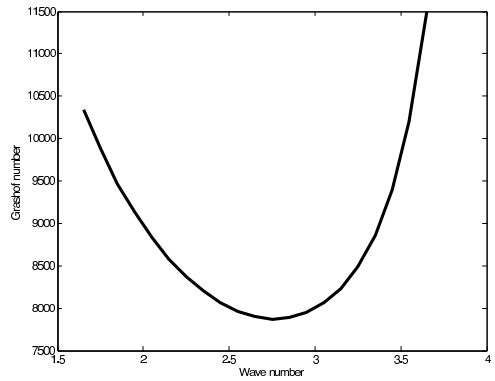

Figure 4: Replication of previous linear stability data for comparison. Curve of neutral stability for pure water corresponding to an eigenvalue, γ, of 0, with minimum corresponding to a critical Grashof number of 7870 at a wavenumber of 2.75. $Pr = 7$, $Le = Ns = 1$, and the buoyancy term in equation (24), $\frac{1}{Ns}D\mathcal{C}$, is set equal to 0. $N = 32$, where N is the number of collocation points.

Investigators	$Gr*$	$m*$	A
Ruth (1979), theory	7868.426	2.767	∞
McBain & Armfield (2003), theory	7868.4264	2.7671	∞
Present Study, theory	7870	2.75	∞

Table 2: Comparison of linear stability results for water at 20°, $Pr = 7$, with values for the parameters critical Grashof number ($Gr*$), associated wavenumber ($m*$), and aspect ratio ($A = L/h$).

We assume a general exponential solution for the perturbation variables ψ', p', T', and C', where the corresponding φ, $\mathcal{P}$, $\mathcal{T}$, and $\mathcal{C}$ are taken to be functions of x only. In general form, with η' representing a dependent variable and ζ representing its corresponding function of x:

$$\eta' = \zeta \exp(i(my + \gamma t)) \tag{21}$$

The nondimensional wavenumber, $m = 1/\text{frequency}$, provides the spatial scale. Physically, values of γ determine the heat-mass transfer regime present: $\gamma < 0$ in the conduction regime, $\gamma = 0$ in the stationary (neutral) case, and $\gamma > 0$ in the convection regime. Because γ is multiplied by i, a positive imaginary γ denotes exponential growth of a perturbation, while a negative imaginary γ denotes its exponential decay. A conceptualized visual representation of the effects of γ upon the fluid flow is given in figure 3.2.

We now incorporate the exponential solution variables into equations (15) - (19). We subtract equation (15) from (16) after applying the operators $imGr$ and DGr, respectively, where D represents the first derivative with respect to x. With some simple rearranging, we obtain:

$$(D^4 - 2m^2D^2 - im\bar{v}GrD^2 + m^4 + im^3\bar{v}Gr + imGrD^2\bar{v})\varphi + D\mathcal{T} + \frac{1}{Ns}D\mathcal{C} = i\gamma Gr(D^2 - m^2)\varphi \tag{22}$$

$$imD\bar{T}GrPr\varphi + (D^2 - m^2 - im\bar{v}GrPr)\mathcal{T} = i\gamma GrPr\mathcal{T} \tag{23}$$

$$imD\bar{C}NsGrLePr\varphi + (D^2 - m^2 - im\bar{v}NsGrLePr)\mathcal{C} = i\gamma NsGrLePr\mathcal{C} \tag{24}$$

Written in matrix form, equations (22) - (24) form the base of our eigenvalue analysis.

4 Chebyshev Collocation Method and Use of MATLAB

4.1 Methods

We will utilize the Chebyshev collocation method detailed by Ehrenstein and Peyret using a MATLAB script. In a general sense, collocation is the process of placing objects (here, functions) side by side or in position. The differential operators, D, in equations (22) - (24) will be evaluated (approximated) by the differentiation of a group of interpolant functions. We discretize the domain along the x-axis into N collocation points, and we let $\{x_j\}_{j=1}^{N}$ be the set of distinct interpolation nodes. By definition, the Chebyshev polynomials are a set of functions, $\{\varphi_j(x_k)\}_{j=1}^{N}$, that satisfy $\varphi_j(x_k) = \delta_{jk}$, where δ_{jk} is the Kronecker delta. Using the Chebyshev polynomials, we can define a discretized polynomial interpolant, $p_{\{N-1\}}(x)$, that is approximately equal to the continuous equations (22) - (24), $f(x)$, at each of the collocation points:

$$p_{\{N-1\}}(x) = \sum_{j=1}^{N} \frac{\alpha(x)}{\alpha(x_j)} \varphi_j(x) f(x_j) \tag{25}$$

We call $p_{\{N-1\}}(x)$ the polynomial interpolant of the original functions. By definition, $\alpha(x)$ is an arbitrary positive weight with at least M continuous derivatives. Here $\alpha(x)$ is designated the coercion function, designed to enforce our specified (Dirichlet or clamped) boundary conditions.

Associated with a function such as (25) is the concept of a differentiation matrix, $\mathbf{D}^{(\ell)}$. Using such matrices, we are able to convert a differential eigenvalue problem into a matrix eigenvalue problem. The operators, $D^\ell = \frac{\partial^\ell}{\partial x^\ell}$, are represented as N x N differentiation matrices with entries:

$$\mathbf{D}_{k,j}^{(\ell)} = \frac{d^\ell}{dx^\ell} \Big[\frac{\alpha(x)}{\alpha(x_j)} \varphi_j(x) \Big]_{x=x_k}, \ell = 1, \ldots, M \tag{26}$$

The MATLAB functions `chebdif` and `cheb4c` as presented by Weideman and Reddy, 2000 define differentiation matrices in our script. The command structure is `[x,D] = chebdif(N,M)` where `D` is an N x N x M array of $\mathbf{D}^{(\ell)}$ matrices, N is the dimension of the matrices, and M is the highest derivative required in the problem. Here, $M = 4$ and N is varied with increasing values of N representing increased precision in our calculations.

In order to solve for the eigenvalues of the system, we must arrange equations (22) - (24) in matrix form:

$$\underbrace{\begin{pmatrix} a11 & a12 & a13 \\ a21 & a22 & a23 \\ a31 & a32 & a33 \end{pmatrix}}_{A} \begin{pmatrix} \varphi \\ \mathcal{T} \\ \mathcal{C} \end{pmatrix} = \gamma \underbrace{\begin{pmatrix} iGr(D^2 - m^2) & 0 & 0 \\ 0 & iGrPr & 0 \\ 0 & 0 & iNsGrLePr \end{pmatrix}}_{B} \begin{pmatrix} \varphi \\ \mathcal{T} \\ \mathcal{C} \end{pmatrix}$$

$$\mathbf{A}\vec{x} = \gamma \mathbf{B}\vec{x} \tag{27}$$

4.2 MATLAB scripts

The MATLAB functions `chebdif` and `cheb4c`, while specifically designed for Dirichlet and clamped boundary conditions, respectively, are designed to work on the domain $[-1, +1]$. Therefore, a set of simple linear transformations of our domain is required in order to effectively employ the `chebdif` and `cheb4c` functions.

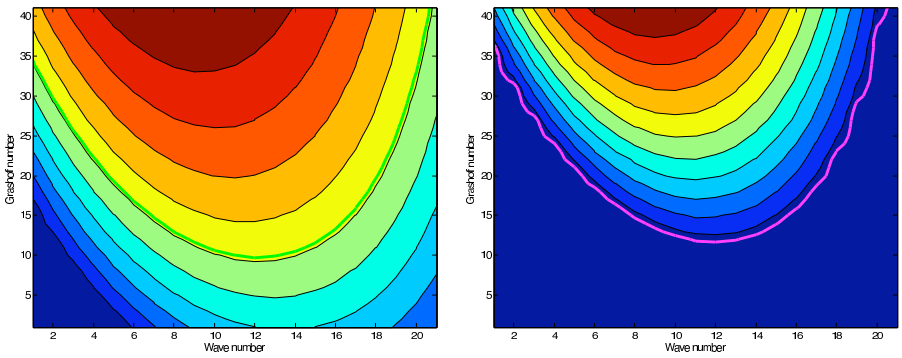

Figure 5: Eigenvalue contours at 0° for (a) pure water, $Pr = 13.183$, and (b) saltwater, $Pr = 13.234$, $Sc = 2654.9$, $Ns = 7.77$. The (a) green or (b) magenta line is the curve of neutral stability corresponding to an eigenvalue, γ, of 0. The labels on the axes represent the number of iterations of the Grashof number and wavenumber within their respective discretized loops, $Gr = [7000 : 100 : 11000]$ and $m = [1.65 : 0.1 : 3.65]$, where the MATLAB command structure is [initial value : increment : final value]. $N = 64$.

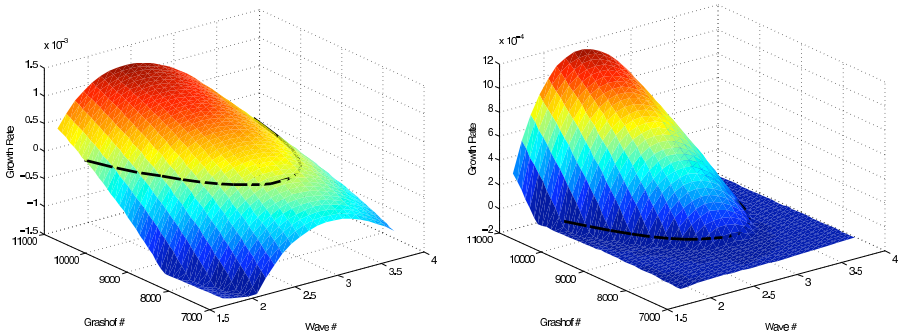

Figure 6: Three-dimensional contour plots for (a) pure water and (b) saltwater following figure 5. In each figure, the black line is the neutral stability curve given as a green or magenta line in figure 5. $N = 64$.

The eigenvalues of the system, γ, are solved using the QR algorithm via the `eig` function in MATLAB solved over loops of the thermal Grashof number and wavenumber for specified values of the fluid parameters Pr, Le or Sc, and Ns for varying levels of precision, N. In our analysis in general, smoother curves are representative of finer sampling within the Gr and m loops.

All scripts adapt Evans code to include concentration, and many stem from a file used to produce an output similar to that of figure 4 for air, $Pr = 0.71$. The critical values given in table 1 under Evans were produced using this script, `psit3.m`, adopted from McBain and Armfield.

In order to be compatible with the current problem, additional transformations of the domain were required. With the exception of the code producing the outputs in figures 7 and 8, the basic structure of the Evans codes remained unchanged.

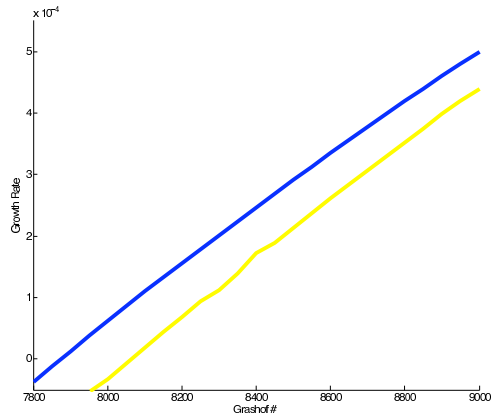

Figure 7: Slice along the Grashof number-growth rate plane in figure 4.2 at the wavenumber of maximal growth. Pure water (figure 6(a)), blue; saltwater (figure 6(b)), yellow. The growth rate increases as the Grashof number increases because the background flow from which perturbations develop is stronger (Evans, 2008). $N = 64$.

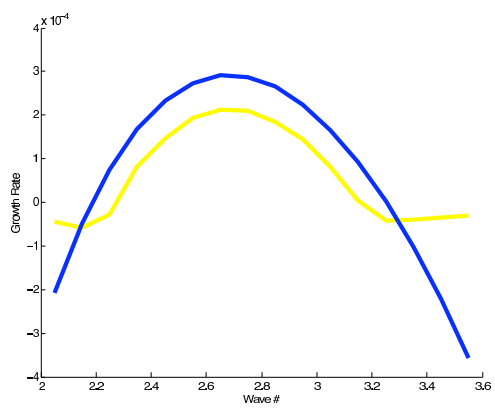

Figure 8: Slice along the wavenumber-growth rate plane in figure 4.2 at $Gr = 8500$. Curves taken at other Grashof numbers weakly unstable to secondary flow growth display a similar relationship. As in figure 7, pure water (figure 6(a)), blue; saltwater (figure 6(b)), yellow. The maxima, $\gamma = 2.91E^{-4}$ at $m = 2.65$ (pure water) and $\gamma = 2.13E^{-4}$ at $m = 2.65$ (saltwater) give the spatial scale of the developing flow patterns. The units of γ are nondimensional seconds^{-1}. $N = 64$.

5 Conclusions

5.1 Discussion

For pure water at 20°, the critical Grashof number and associated wavenumber results of 7870 and 2.75 as plotted in figure 4 closely match the values found by Ruth and McBain and Armfield, providing significant validation for the base case of water as the fluid in the model. See table 3.3.

At 0°, the ice-saltwater specific parameter combination of $Pr = 13.234$, $Sc = 2654.9$, $Ns = 7.77$ (Kukulka et al., 1987), provided the critical result $Gr* = 8070$ at $m* = 2.75$, well within a physically reasonable range. At the same temperature, the pure water parameter combination of $Pr = 13.183$ (Kukulka et al., 1987), $Le = Ns = 1$ with the buoyancy force term due to concentration in equation (22) set equal to 0, provided the critical result $Gr* = 7880$ at $m* = 2.75$. Because we assume similar fluid properties, we expect the wavenumbers to be similar; in this case, they are identical.

We expect the critical Grashof number to be somewhat higher in saltwater than in pure water at the same temperature. Alone, the buoyancy force resulting from our salinity gradient, $C = [0, +0.5]$, would create a clockwise flow within the box model: in the primary shear flow, less salted, lighter particles from the left of the cavity would rise while more heavily salted, more dense particles toward the right of the cavity would fall. Thus, the salinity buoyancy force opposes the destabilizing temperature buoyancy force depicted in figure 2. Therefore, in the terms of a buoyancy force among the many complexities of the fluid flow, the addition of a salinity gradient supplies stability to the model and increases the critical Grashof number required for the presence of secondary flows.

In three dimensions (Grashof number, wavenumber, growth rate), the pure water and saltwater cases at 0° are compared. In a physical sense, over the duration of the melting of an ice sheet, the behavior of the fluid initially assumed to be saltwater tends toward that of pure water as freshwater from the surrounding ice dilutes the fluid, providing motivation for such a comparison.

The growth rate data given in figures 7 and 8 confirms the prediction that the addition of a salinity gradient provides stability to the model. In figure 7, we note that the transition between laminar and turbulent flow occurs a significantly higher Grashof number in saltwater (yellow) than in pure water (blue). Even when secondary flows may develop in saltwater, they do so at a significantly lower growth rate in comparison to their pure water counterparts. In figure 8, the same smaller growth rate trend is shown for one value of the Grashof number, $Gr = 8500$. Further, on the edges of the domain where the growth rate is below zero, secondary flows in salt water decay much less precipitously than their pure water counterparts. Figure 8 also clearly displays the similarities in spatial scale of the secondary flows found in pure water (blue) and saltwater (yellow).

5.2 Implications

This work could provide an independent test to PDE solution models. A nonlinear solution method employing the JFNK algorithm will examine the development of secondary flows and use the present work as a comparison (Evans, 2008).

The study of small scale flows is an important component of climate research and modeling today. Even the best of today's models use a grid spacing of around 20 km; flows such as those examined in the present study are invisible in such a model. Accuracy of current models as well as knowledge of when assumptions made in global models may become unreasonable can be improved through the study of small scale flows.

However small, the implications of such a flow can be significant. Convection is a much more efficient method of heat transfer than conduction, and the study of the transition between the two is important to understanding the possible consequences accelerated attenuation of ice such a flow can create.

The author would like to thank research mentor Katherine J. Evans (Kate), without whom this project would not have been possible. This work was completed as a part of the Research Alliance in Math and Science (RAMS) program, sponsored by the Office of Advanced Scientific Computing Research, U.S. Department of Energy, at UT-Battelle, LLC-managed Oak Ridge National Laboratory under Contract No. De-AC05-00OR22725, Subcontract No. 4000069838. This work has been authored by a subcontractor of the U.S. Government; accordingly, the U.S. Government retains a non-exclusive, royalty-free license to publish or reproduce the published form of this contribution or allow others to do so, for U.S. Government purposes.

References

Batchelor, G. (1954). Heat transfer by free convection across a closed cavity between vertical boundaries at different temperatures. *Q. Appl. Math.*, 12(3):209–233.

Bennacer, R., Mohamad, A. A., and Akrour, D. (2001). Transient natural convection in an enclosure with horizontal temperature and vertical solutal gradients. *Int. J. Therm. Sci.*, 40:899–910.

Bergholz, R. F. (1978). Instability of steady natural convection in a vertical fluid layer. *J. Fluid Mech.*, 84:743–768.

Ehrenstein, U. and Peyret, R. (1989). A chebyshev collocation method for the navier-stokes equations with application to double-diffusive convection. *Int. J. Numer. Methods Fluids*, 9:427–452.

Evans, K. (2008). Linear stability analysis as a temporal accuracy benchmark. To be submitted.

Hadji, L. and Jin, X.-X. (1996). Penetrative convection induced by the freezing of seawater. *Int. J. Heat Mass Transfer*, 39(18):3823–3834.

Inc., T. M. (2007). Matlab 7.4. licensed under Dartmouth College.

Josberger, E. G. and Martin, S. (1981). A laboratory and theoretical study of the boundary layer adjacent to a vertical melting ice wall in salt water. *J. Fluid Mech.*, 111:439–473.

Kukulka, D. J., Gebhart, G., and Mollendorf, J. C. (1987). Thermodynamic and transport properties of pure and saline water. *Adv. Heat Transfer*, 18:325–363.

Lauriat, G. and Desrayaud, G. (1985). Natural convection in air-filled cavities of high aspect ratios: Discrepancies between experimental and theoretical results. *ASME Paper 85-HT-37*.

Mamou, M., Vasseur, P., and Hasnaoui, M. (2001). On numerical stability analysis of double-diffusive convection in confined enclosures. *J. Fluid Mech.*, 433:209–250.

McBain, G. and Armfield, S. (2003). Natural convection in a vertical slot: accurate solution of the linear stability equations. Sydney, NSW. Eleventh Computational Techniques and Applications Conference, Fifth International Congress on Industrial and Applied Mathematics.

McBain, G. and Armfield, S. (2004). Natural convection in a vertical slot: accurate solution of the linear stability equations. *ANZIAM J.*, 45:C92–C105.

Mergui, S. and Gobin, D. (2000). Transient double diffusive convection in a vertical enclosure with aymmetrical boundary conditions. *J. Heat Transfer*, 122:598–602.

Petrich, C., Langhorne, P. J., and Haskell, T. G. (2007). Formation and structure of refrozen cracks in land-fast first-year sea ice. *J. Geophys. Res.*, 112.

Quon, C. and Ghil, M. (1992). Multiple equilibria in thermosolutal convection due to salt-flux boundary conditions. *J. Fluid Mech.*, 245:449–483.

Ruth, D. (1979). On the transition to transverse rolls in an infinite vertical fluid layer–a power series solution. *Int. J. Heat Mass Transfer*, 22:1199–1208.

Vest, C. M. and Arpaci, V. S. (1969). Stability of natural convection in a vertical slot. *J. Fluid Mech.*, 36:1–15.

Weideman, J. and Reddy, S. (2000). A matlab differentiation matrix suite. *ACM Transactions on Mathematical Software*, 26(4):465–519.